Available online at www.sciencedirect.com
ScienceDirect
Journal of Sound and Vibration 323 (2009) 1032–1044
JOURNAL OF SOUND AND VIBRATION
www.elsevier.com/locate/jsvi

Transmission loss analysis of rectangular expansion chamber with arbitrary location of inlet/outlet by means of Green's functions

B. Venkatesham[b], Mayank Tiwari[b], M.L. Munjal[a,*]

[a]*Facility for Research in Technical Acoustics (FRITA), Department of Mechanical Engineering, Indian Institute of Science, Bangalore 560012, India*
[b]*GE, Global Research, Bangalore, India*

Received 2 September 2008; received in revised form 12 January 2009; accepted 19 January 2009
Handling Editor: J. Lam
Available online 28 February 2009

Abstract

Transmission loss of a rectangular expansion chamber, the inlet and outlet of which are situated at arbitrary locations of the chamber, i.e., the side wall or the face of the chamber, are analyzed here based on the Green's function of a rectangular cavity with homogeneous boundary conditions. The rectangular chamber Green's function is expressed in terms of a finite number of rigid rectangular cavity mode shapes. The inlet and outlet ports are modeled as uniform velocity pistons. If the size of the piston is small compared to wavelength, then the plane wave excitation is a valid assumption. The velocity potential inside the chamber is expressed by superimposing the velocity potentials of two different configurations. The first configuration is a piston source at the inlet port and a rigid termination at the outlet, and the second one is a piston at the outlet with a rigid termination at the inlet. Pressure inside the chamber is derived from velocity potentials using linear momentum equation. The average pressure acting on the pistons at the inlet and outlet locations is estimated by integrating the acoustic pressure over the piston area in the two constituent configurations. The transfer matrix is derived from the average pressure values and thence the transmission loss is calculated. The results are verified against those in the literature where use has been made of modal expansions and also numerical models (FEM fluid). The transfer matrix formulation for yielding wall rectangular chambers has been derived incorporating the structural–acoustic coupling. Parametric studies are conducted for different inlet and outlet configurations, and the various phenomena occurring in the TL curves that cannot be explained by the classical plane wave theory, are discussed.

1. Introduction

Rectangular expansion chamber silencers are extensively used in HVAC ducts as a plenum chamber and other industrial applications. Four-pole parameters are very useful for the analysis of complex HVAC system with different duct configurations.

*Corresponding author. Tel.: +91 80 2293 2303; fax: +91 80 23600648.
E-mail address: munjal@mecheng.iisc.ernet.in (M.L. Munjal).

0022-460X/$ - see front matter © 2009 Elsevier Ltd. All rights reserved.
doi:10.1016/j.jsv.2009.01.035

Munjal [1] discussed the basic concepts of the four-pole parameters and derived them for different silencer elements mostly in the range of plane waves with rigid wall configurations. Kim and Soedel [2] derived a generalized transfer matrix formulation from the pressure response solution including higher-order modes. They mentioned that this approach is applicable provided the correct pressure response solution is known, and demonstrated this method for an annular cylinder using a point source excitation. There might be a numerical convergence problem near the point source location and this could be overcome by a piston source modeling.

Kim and Kang [3] gave a general formulation to derive the transfer matrix based on Green's functions for a circular expansion chamber with arbitrary locations of inlet, outlet port, termination conditions, and validated the results with experiments. Ih [4] discussed the transfer matrix formulation for different configurations of rectangular plenum chamber using the modal expansion method and validated the same with available literature. He used Munjal's collocation method [5] to validate the centered-inlet and outlet configuration.

The present paper discusses the same problem as in Ref. [4] using Green's function to calculate the inside pressure field. The current analytical formulation incorporates not only the rigid walls chambers but also the ones with yielding walls. The assumptions involved in the formulation are: no mean flow and no acoustic source inside the plenum chamber. The Green's function approach has an advantage in modeling the absorptive boundary conditions and also flexible walls. The rectangular expansion chamber is modeled as a piston-driven rectangular cavity where the pistons are fluctuating in a predetermined manner. The four-pole parameters are explicitly given in a very simple form using Green's function of the rectangular cavity in terms of a finite number of modes. Initially, the four-pole parameters of the offset inlet and outlet configuration are derived. The four-pole parameters of the other inlet/outlet configurations are adopted from the offset configuration without further calculations. A transfer matrix formulation has been developed for the yielding wall rectangular chamber by considering the structural–acoustic coupling. The transfer matrix so derived may be combined with the transfer matrices of the muffler or system elements upstream and downstream in order to predict the overall TL of the system.

2. Theoretical formulation

2.1. Green's function derivation

Fig. 1 shows the schematic diagram of a simple rectangular expansion chamber with different inlet and outlet configurations. If the dimensions of the inlet and outlet port were small compared to wavelength, then the uniform velocity assumption would be valid. Green's function for rectangular cavity in terms of the cavity mode shapes is given by [6]

$$G(\vec{x}|\vec{x}_0) = \sum_{mpn} \frac{\bar{\psi}_{mpn}(\vec{x})\psi_{mpn}(\vec{x}_0)}{k_{mpn}^2 - k^2}. \tag{1}$$

Here, $k = \omega/c_0$ is the wavenumber, and the mode shape of a rectangular cavity is given by [6]

$$\psi_{mpn}(\vec{x}) = \cos\frac{m\pi x}{a}\cos\frac{p\pi y}{l}\cos\frac{n\pi z}{b}, \tag{2}$$

with the corresponding wavenumber and the natural frequency as

$$k_{mpn} = \left[\left(\frac{m\pi}{a}\right)^2 + \left(\frac{p\pi}{l}\right)^2 + \left(\frac{n\pi}{b}\right)^2\right]^{1/2}, \tag{3}$$

and

$$\omega_{mpn} = \pi c_0\left[\left(\frac{m}{a}\right)^2 + \left(\frac{p}{l}\right)^2 + \left(\frac{n}{b}\right)^2\right]^{1/2}, \tag{4}$$

and the orthonormal function $\bar{\psi}_{mpn}(\vec{x})$ is written as

$$\bar{\psi}_{mpn}(\vec{x}) = \frac{e_m e_p e_n}{V}\psi_{mpn}(\vec{x}). \tag{5}$$

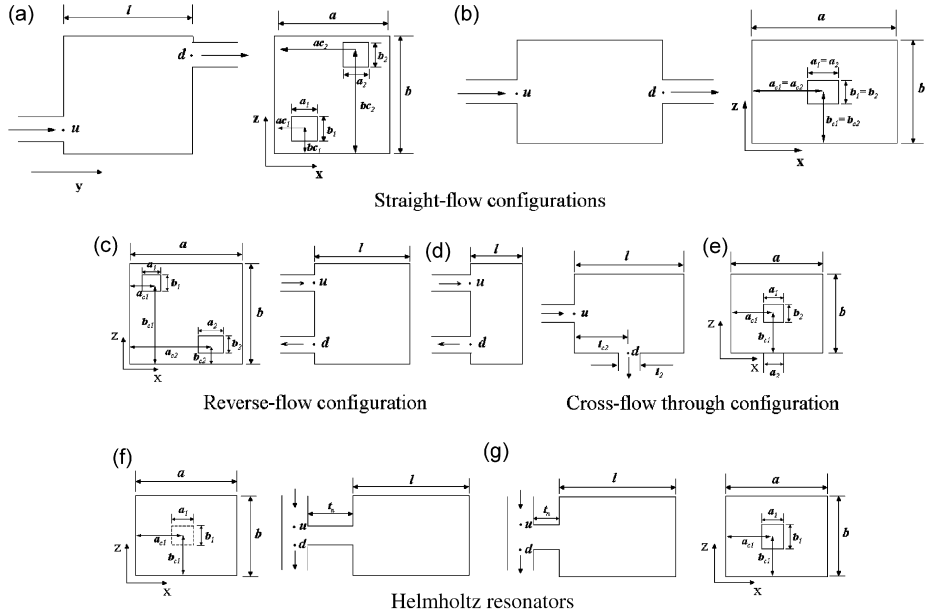

Fig. 1. Schematic diagram of rectangular expansion chamber with different inlet and outlet configurations: (a) offset inlet, outlet (two views); (b) centered inlet, outlet; (c) reverse flow expansion with long end-chamber; (d) reverse flow expansion with short end-chamber; (e) end-in, side-out chamber; (f) long neck Helmholtz-resonator; and (g) short neck Helmholtz-resonator.

Here, $\vec{x}$ and $\vec{x}_0$ are the response coordinates vector and source coordinates vector, respectively; n, p and m are integers; a, l and b are dimensions (in m) of the rectangular expansion chamber in the x, y and z coordinate directions, as shown in Fig. 1a; and V is volume of the chamber ($V = alb$). The normalization factors are given by $e_m = 1$ if $m = 0$ and $e_m = 2$ if $m \geqslant 1$, $e_n = 1$ if $n = 0$ and $e_n = 2$ if $n \geqslant 1$, $e_p = 1$ if $p = 0$ and $e_p = 2$ if $p \geqslant 1$; and c_0 is speed of sound in m/s.

Substituting Eq. (5) into Eq. (1) yields

$$G(\vec{x}|\vec{x}_0) = \sum_{mpn} \frac{e_m e_p e_n}{V} \frac{\psi_{mpn}(\vec{x})\psi_{mpn}(\vec{x}_0)}{k_{mpn}^2 - k^2}. \tag{6}$$

The acoustic wave equation that determines the acoustic field in the rectangular chamber can be expressed as [6]

$$\nabla^2\phi + k^2\phi = -Q(\vec{x}), \tag{7}$$

where Q is the embedded source, if any, for the sake of generality.

Assuming harmonic time behavior, the velocity potential may be written as $\phi(\vec{x}, t) = \phi(\vec{x})e^{j\omega t}$.

Thus, acoustic pressure

$$p(\vec{x}, t) = -\rho \frac{\partial\phi(\vec{x}, t)}{\partial t} = -\rho j\omega\phi(\vec{x}) \tag{8}$$

and particle velocity

$$u(\vec{x}) = \text{grad}\,\phi(\vec{x}) = \nabla\phi(\vec{x}). \tag{9}$$

2.2. Derivation of the velocity potential

Total velocity potential inside the chamber is expressed by superimposing the velocity potentials generated due to the inlet and outlet piston sources. Thus, the expression for total velocity potential can

be written as [3]

$$\phi(\vec{x}) = -\left[\int\int G(\vec{x}|\vec{x}_0)N_1(x_0,z_0)\,ds_A + \int\int G(\vec{x}|\vec{x}_0)N_2(x_0,z_0)\,ds_A\right]. \tag{10}$$

Let us assume

$$\phi_1(\vec{x}) = -\int\int_{piston1} G(\vec{x}|\vec{x}_0)N_1(x_0,z_0)\,dx\,dz \tag{11a}$$

and

$$\phi_2(\vec{x}) = -\int\int_{piston2} G(\vec{x}|\vec{x}_0)N_2(x_0,z_0)\,dx\,dz, \tag{11b}$$

where

$$N_1(x_0,z_0) = u_1\left[H\left\{x-\left(ac_1-\frac{a_1}{2}\right)\right\} - H\left\{x-\left(ac_1+\frac{a_1}{2}\right)\right\}\right]\left[H\left\{z-\left(bc_1-\frac{b_1}{2}\right)\right\} - H\left\{z-\left(bc_1+\frac{b_1}{2}\right)\right\}\right] \equiv u_1 f_1(x_0,z_0), \tag{11c}$$

$$N_2(x_0,z_0) = u_2\left[H\left\{x-\left(ac_2-\frac{a_2}{2}\right)\right\} - H\left\{x-\left(ac_2+\frac{a_2}{2}\right)\right\}\right]\left[H\left\{z-\left(bc_2-\frac{b_2}{2}\right)\right\} - H\left\{z-\left(bc_2+\frac{b_2}{2}\right)\right\}\right] \equiv u_2 f_2(x_0,z_0). \tag{11d}$$

Here, H $(\cdot)$ is Heaviside function, and u_1 and u_2 are velocities of the hypothetical pistons at the inlet and outlet, respectively.

Substituting the Green's function expression (6) into Eq. (11a) gives

$$\phi_1(x,y,z) = -\int_{b_{c1}-b_1/2}^{b_{c1}+b_1/2}\int_{a_{c1}-a_1/2}^{a_{c1}+a_1/2}\sum_{mpn}\frac{e_m e_p e_n}{V}\frac{\psi_{mpn}(x,y,z)}{k_{mpn}^2-k^2}\psi_{mpn}(x_0,y_0,z_0)u_1 f_1(x_0,z_0)\,dx_0\,dz_0 \tag{12}$$

$$= -u_1\sum_{mpn}\frac{e_m e_p e_n}{V}\frac{\psi_{mpn}(\vec{x})}{k_{mpn}^2-k^2}\left[\cos\frac{p\pi y_0}{l}\,C_{m1}C_{n1}\right], \tag{13}$$

where

$$C_{m1} = \begin{cases} a_1 & \text{for } m=0 \\ \dfrac{2a}{m\pi}\cos\left(\dfrac{m\pi a_{c1}}{a}\right)\sin\left(\dfrac{m\pi a_1}{2a}\right) & \text{for } m\neq 0 \end{cases} \tag{14a}$$

and

$$C_{n1} = \begin{cases} b_1 & \text{for } n=0 \\ \dfrac{2b}{n\pi}\cos\left(\dfrac{n\pi b_{c1}}{b}\right)\sin\left(\dfrac{n\pi b_1}{2b}\right) & \text{for } n\neq 0 \end{cases}. \tag{14b}$$

Similarly, velocity potential ϕ_2 due to the piston source at the outlet may be obtained. Generalizing the results, the velocity potential caused by port i can be written as

$$\phi_i(\vec{x}) = \sum_{mpn} S_{mpn}^i \psi_{mpn}(\vec{x}), \tag{15}$$

where

$$S^{i}_{mpn} = \frac{(-1)^{i} e_m e_p e_n \cos(p\pi y_{io}/l)}{k^2_{mpn} - k^2} \frac{C_{mi} C_{ni} u_i}{V} \tag{16}$$

and ψ_{mpn} is given by Eq. (2), and C_{mi}, C_{ni} are given by Eq. (14), with subscript 1 being replaced by i; where $i = 1$ and 2.

2.3. The transfer matrix derivation

The transmission loss of the chamber, which expresses the performance of the rectangular chamber, can be obtained from the four-pole parameters, which in turn may be derived from the velocity potentials. Making use of Eq. (8), acoustic pressure is written as $p_i = -j\omega\rho_0\phi_i(\vec{x})$.

The average sound pressure acting on the piston "i" with cross-sectional area "A_i" by the velocity field, which is generated by the rectangular piston "i'", can be written as

$$\bar{p}_{ii'} = -\frac{j\omega\rho_0}{A_i} \int\int_{piston\ i} \phi_{i'}(\vec{x})\, ds_i \tag{17}$$

or

$$\bar{p}_{ii'} = \frac{-j\omega\rho_0}{A_i} \int_{a_{ci}-a_i/2}^{a_{ci}+a_i/2} \int_{b_{ci}-b_i/2}^{b_{ci}+b_i/2} \phi_{i'}\, dz\, dx. \tag{18}$$

Substituting Eq. (15) into Eq. (18) gives

$$\bar{p}_{ii'} = \frac{-j\omega\rho_0}{A_i} \int_{a_{ci}-a_i/2}^{a_{ci}+a_i/2} \int_{b_{ci}-b_i/2}^{b_{ci}+b_i/2} \sum_{mpn} S^{i'}_{mpn} \psi_{mpn}(\vec{x})\, dz\, dx. \tag{19}$$

Substituting Eq. (16) into Eq. (19) gives

$$\bar{p}_{ii'} = (-1)^{i'} \frac{j\omega\rho_0 u_{i'}}{A_i} \sum_{mpn} \frac{e_m e_p e_n}{V} \cdot \frac{(-1)}{k^2_{mpn} - k^2} \cos\left(\frac{p\pi y_{i'o}}{l}\right) \cos\left(\frac{p\pi y_{io}}{l}\right) C_{mi'} C_{ni'} C_{mi} C_{ni}. \tag{20}$$

By rearranging the terms, it can be expressed as

$$\bar{p}_{ii'} = \frac{(-1)^{i'}}{A_i A_{i'}} \cdot jZ_0 v_{i'} \sum_{mpn} \frac{e_m e_p e_n}{l} \cdot \left(\frac{-k}{k^2_{mpn} - k^2}\right) \cos\left(\frac{p\pi y_{i'o}}{l}\right) \cos\left(\frac{p\pi y_{io}}{l}\right) C_{mi'} C_{ni'} C_{mi} C_{ni}. \tag{21}$$

Here, $Z_0 = \rho_0 c_0 / S$ is the characteristic impedance of the chamber, ρ_0 the air density, c_0 the speed of sound, and $S = ab$ the cross-sectional area of the chamber.

Defining the volume velocity $v_i = A_i u_i$, and

$$E_{ii'} \equiv \frac{-1}{A_i A_{i'}} \sum_{mpn} \frac{e_m e_p e_n}{l} \cdot \left(\frac{k}{k^2_{mpn} - k^2}\right) \cos\left(\frac{p\pi y_{i'o}}{l}\right) \cos\left(\frac{p\pi y_{io}}{l}\right) C_{mi'} C_{ni'} C_{mi} C_{ni}, \tag{22}$$

the averaged acoustic pressures on the surfaces of the two "pistons" may be written as

$$\bar{p}_{ii'} = (-1)^{i'} jZ_0 v_{i'} E_{ii'}. \tag{23}$$

For the condition $i = i'$ Eq. (22) reduces to

$$E_{ii} = \frac{-1}{A_i^2} \sum_{mpn} \frac{e_m e_p e_n}{l} \cdot \left(\frac{k}{k^2_{mpn} - k^2}\right) \cos^2\left(\frac{p\pi y_{io}}{l}\right) C^2_{mi} C^2_{ni}, \quad i = 1 \text{ or } 2. \tag{24}$$

From Eq. (22) it may be noted that $E_{ii'} = E_{i'i}$, which shows that these values are independent of the inlet and outlet port (or piston) positions. In other words, E-functions satisfy the reciprocity principle.

The total sound pressure acting on the inlet and outlet ports or pistons can be expressed as

$$\bar{p}_1 = \bar{p}_{11} + \bar{p}_{12} = -jv_1 Z_0 E_{11} + jv_2 Z_0 E_{12} \tag{25a}$$

and

$$\bar{p}_2 = \bar{p}_{22} + \bar{p}_{21} = jv_2 Z_0 E_{22} - jv_1 Z_0 E_{21}. \tag{25b}$$

The transfer matrix of the rectangular expansion chamber of Fig. 1a, relating the acoustic state variables at the inlet and outlet may now be written as

$$\begin{bmatrix} \bar{p}_1 \\ v_1 \end{bmatrix} = \begin{bmatrix} T_{11} & T_{12} \\ T_{21} & T_{22} \end{bmatrix} \begin{bmatrix} \bar{p}_2 \\ v_2 \end{bmatrix}. \tag{26}$$

Making use of Eq. (25), the four-pole parameters $T_{ii'}$ can be written in terms of the E-functions as follows [4]:

$$T_{11} = \left(\frac{\bar{p}_1}{\bar{p}_2}\right)_{v_2=0} = \frac{E_{11}}{E_{12}}, \tag{27a}$$

$$T_{12} = \left(\frac{\bar{p}_1}{v_2}\right)_{\bar{p}_2=0} = jZ_0\left(E_{12} - \frac{E_{11}E_{22}}{E_{12}}\right), \tag{27b}$$

$$T_{21} = \left(\frac{v_1}{\bar{p}_2}\right)_{v_2=0} = j(Z_0 E_{12})^{-1}, \tag{27c}$$

$$T_{22} = \left(\frac{v_1}{v_2}\right)_{\bar{p}_2=0} = \frac{E_{22}}{E_{12}}. \tag{27d}$$

The transmission loss can be expressed in terms of the four-pole parameters as [1]

$$TL = 20\log_{10}\{(Z_2/Z_1)^{1/2}|T_{11} + T_{12}/Z_2 + T_{21}Z_1 + T_{22}(Z_1/Z_2)|/2\}, \tag{28}$$

where Z_1 and Z_2 are characteristic impedances of the inlet duct and outlet duct, respectively: $Z_1 = \rho_0 c_0/S_1$ and $Z_2 = \rho_0 c_0/S_2$, where $S_1 = a_1 b_1$ and $S_2 = a_2 b_2$.

2.4. Straight-flow configurations

The configurations shown in Figs. 1a and b are the straight-flow configurations. Generally, in this configuration the inlet and outlet port openings face each other. The quantities required to calculate the four-pole parameters of the straight-flow configuration in Figs. 1a and b can be deduced from Eqs. (22) and (24) as

$$E_{11} = \frac{-1}{(a_1 b_1)^2}\sum_{mpn}\frac{e_m e_p e_n}{l}\cdot\left(\frac{k}{k_{mpn}^2 - k^2}\right)C_{m1}^2 C_{n1}^2, \tag{29a}$$

$$E_{12} = E_{21} = \frac{-1}{(a_1 b_1)(a_2 b_2)}\sum_{mpn}\frac{e_m e_p e_n}{l}\cdot\left(\frac{k}{k_{mpn}^2 - k^2}\right)C_{m1} C_{m2} C_{n1} C_{n2}(-1)^p, \tag{29b}$$

$$E_{22} = \frac{-1}{(a_2 b_2)^2}\sum_{mpn}\frac{e_m e_p e_n}{l}\cdot\left(\frac{k}{k_{mpn}^2 - k^2}\right)C_{m2}^2 C_{n2}^2. \tag{29c}$$

2.5. Reverse-flow configuration

Generally in this configuration the inlet and outlet ports are on the same face and the flow direction is reversed as shown in Figs. 1c and d. The quantities required to calculate the four-pole parameters in the

reverse flow are E_{11}, E_{12} and E_{22}. Expressions for E_{11} and E_{22} are the same as for the straight-flow configurations. E_{12} is obtained from Eq. (22) as

$$E_{12} = \frac{-1}{(a_1 b_1)(a_2 b_2)} \sum_{mpn} \frac{e_m e_p e_n}{l} \left(\frac{k}{k_{mpn}^2 - k^2} \right) C_{m1} C_{m2} C_{n1} C_{n2}. \tag{30}$$

2.6. The end-in side-out configuration (EISO)

Fig. 1e shows the EISO cross-flow configuration. Generally in this configuration, inlet and outlet port are in the mutually perpendicular faces. The quantity required to calculate the four-pole parameter, E_{11}, is the same as for the straight-flow configuration, and the remaining quantities E_{12} and E_{22} are expressed by replacing b_2 with rectangular piston width l_2 in the reverse-flow configuration E_{12} and E_{22}:

$$E_{12} = \sum_{mpn} \frac{-1}{(a_1 b_1 a_2 l_2)} \frac{e_m e_p e_n}{l} \left(\frac{k}{k_{mpn}^2 - k^2} \right) (C_{m1} C_{m2} C_{n1} C_{n2}) \tag{31a}$$

and

$$E_{22} = \sum_{mpn} \frac{-1}{(a_2 l_2)^2} \frac{e_m e_p e_n}{l} \left(\frac{k}{k_{mpn}^2 - k^2} \right) (C_{m2} C_{n2})^2. \tag{31b}$$

2.7. Helmholtz resonators

The four-pole parameters for Helmholtz resonator (Figs. 1f and g) are expressed as [3]

$$T_{11} = 1, \tag{32a}$$

$$T_{12} = 0, \tag{32b}$$

$$T_{21} = \frac{j}{\left(Z_0 E_{11} - \dfrac{S\omega t_n}{a_1 b_1} \right)}, \tag{32c}$$

$$T_{22} = 1. \tag{32d}$$

Here, acoustic inertance of the neck $S\omega t_n/a_1 b_1$ is added to the compliance of chamber volume in the four-pole parameters T_{21} of Helmholtz-resonator. $S = ab$, and a_1 and b_1 are cross-dimensions of the neck. E_{11} represents the self-inertance and it is identical to E_{11} in the straight-flow configuration (see Eq. (29a)).

2.8. Rectangular chamber with yielding wall

The sound field inside the chamber is through the imposed surface piston source and coupling between acoustic space and flexible wall. A strong coupling is assumed between the chamber and the flexible plate, and a weak coupling between the flexible plate and the outside radiated acoustic field.

General equations of the inside expansion chamber pressure p at location $\mathbf{x}$ and the compliant wall vibration velocity w at location $\mathbf{z}$ on the flexible plate for the uncoupled cavity modes N and structural modes M are

$$p(\mathbf{x}, \omega) = \sum_{n=1}^{N} \psi_n(\mathbf{x}) a_n(\omega) = \boldsymbol{\psi}^{\mathrm{T}} \mathbf{a} \tag{33a}$$

and

$$w(\mathbf{z},\omega)=\sum_{m=1}^{M}\phi_m(\mathbf{z})b_m(\omega)=\mathbf{\Phi}^T\mathbf{b}, \tag{33b}$$

where $\psi_n(\mathbf{x})$ is the uncoupled acoustic mode shape function, $a_n(\omega)$ is the complex amplitude of the nth acoustic pressure mode, $\phi_m(\mathbf{z})$ is the uncoupled vibration mode shape function, and $b_m(\omega)$ is the complex amplitude of the mth vibration velocity mode.

The structural mode shape function for a simply supported rectangular plate normalized by its surface area is [7]

$$\phi_m(\mathbf{z})=2\,\sin\left(\frac{m_1\pi x}{L_1}\right)\sin\left(\frac{m_2\pi y}{L_2}\right), \tag{34}$$

where m_1 and m_2 are mode numbers with positive integers.

The modal acoustic pressure vector $\mathbf{a}$ can be expressed in the matrix form as

$$\mathbf{a}=\mathbf{Z_a}(\mathbf{q}+\mathbf{q_s}), \tag{35}$$

where $\mathbf{Z_a}=\mathbf{A}\rho_\mathbf{0}c_0^2/V$ is an $(N\times N)$ diagonal matrix defined as the uncoupled acoustic modal impedance matrix: $\mathbf{q_s}=\mathbf{Cb;}$ $\mathbf{q}$ is the N length modal source strength vector, and $\mathbf{q_s}$ is the modal source vector due to vibration of the structure. Matrix $\mathbf{A}$ is an $(N\times N)$ diagonal matrix. It contains acoustic mode resonance terms [7]. $\mathbf{C}$ is an $(N\times M)$ matrix defined as coupling coefficient between nth acoustic mode and mth structural mode.

The modal vibration amplitude vector $\mathbf{b}$ can be expressed in the matrix form as

$$\mathbf{b}=\mathbf{Y_s}(\mathbf{g}-\mathbf{g_a}) \tag{36a}$$

$$\mathbf{g_a}=\mathbf{C^T}\mathbf{a} \tag{36b}$$

where $\mathbf{g}$ is the generalized modal force vector due to the external force distribution, $\mathbf{g_a}$ is the modal force vector acting on the acoustic system, $\mathbf{Y_s}=B/(\rho_s h S_f)$ is the $(M\times M)$ diagonal matrix defined as the uncoupled structural modal mobility matrix, B is an $(M\times M)$ diagonal matrix consisting of structural mode resonance term, ρ_s and h denote density of the plate material and thickness of the plate, respectively.

Combining Eqs. (35) and (36a) yields the acoustic and structural modal amplitude vectors $\mathbf{a}$ and $\mathbf{b}$ in terms of the modal excitation vectors $\mathbf{q}$ and $\mathbf{g}$:

$$\mathbf{a}=(\mathbf{I}+\mathbf{Z_a}\mathbf{C}\mathbf{Y_s}\mathbf{C^T})^{-1}\mathbf{Z_a}(\mathbf{q}+\mathbf{C}\mathbf{Y_s}\mathbf{g}), \tag{37a}$$

$$\mathbf{b}=(\mathbf{I}+\mathbf{Y_s}\mathbf{C^T}\mathbf{Z_a}\mathbf{C})^{-1}\mathbf{Y_s}(\mathbf{g}-\mathbf{C^T}\mathbf{Z_a}\mathbf{q}). \tag{37b}$$

Substituting pressure equation into Eq. (17) gives

$$\bar{p}_{ii'}=\frac{1}{A_i}\int\int_{piston\ i}\sum_{n=1}^{N}a_{n,i'}\psi_n(\vec{x})\,ds_i. \tag{38}$$

Substituting Eq. (2) into Eq. (38) and after simplification, it can be written as

$$\bar{p}_{ii'}=\frac{\mathbf{q_i^T}\mathbf{a}_{i'}}{A_i}, \tag{39a}$$

where rth element of vector $\mathbf{q_i}$ for the (m, p, n) mode is given by

$$q_{r,i}=C_{mi}C_{ni}\,\cos\left(\frac{p\pi y_i}{l}\right). \tag{39b}$$

C_{mi} and C_{ni} are given in Eqs. (14a) and (14b), respectively. Assuming a unit particle velocity piston source and the E-function, the four-pole parameters in Eqs. (26) for a rectangular expansion chamber are expressed

as under:

$$E_{11} = \frac{\mathbf{j}\mathbf{q}_1^{\mathrm{T}}\mathbf{a}_1}{Z_0(a_1b_1)^2}, \tag{40}$$

$$E_{21} = E_{12} = \left(\frac{j}{Z_0}\right)\frac{\mathbf{q}_1^{\mathrm{T}}\mathbf{a}_2}{(a_1b_1a_2b_2)}, \tag{41}$$

$$E_{22} = \left(\frac{j}{Z_0}\right)\frac{\mathbf{q}_2^{\mathrm{T}}\mathbf{a}_2}{(a_2b_2)^2}. \tag{42}$$

The proposed analytical formulation for yielding walls is applied to a rectangular expansion chamber with a simple supported flexible wall. The dimensions of the chamber are: $a = b = 0.15\,\mathrm{m}$, $a_1 = b_1 = a_2 = b_2 = 0.05\,\mathrm{m}$, $a_{c1} = b_{c1} = a_{c2} = b_{c2} = 0.125\,\mathrm{m}$, and wall thickness $= 0.001\,\mathrm{m}$. Materials properties used in the analytical calculations are: density $= 2770\,\mathrm{kg/m^3}$, Young's modulus $= 71 \times 10^9\,\mathrm{N/m^2}$, and Poisson's ratio $= 0.33$.

3. Numerical model

An FEM based numerical model has been used here to validate and compare the computational time between the analytical model and the numerical model. The "FEM fluid" analysis has been performed in the commercial package named SYSNOISE [8]. A simple rectangular expansion chamber as shown in Fig. 1b with dimensions of $a = b = 0.15\,\mathrm{m}$, $a_1 = b_1 = a_2 = b_2 = 0.05\,\mathrm{m}$, $a_{c1} = b_{c1} = a_{c2} = b_{c2} = 0.125\,\mathrm{m}$. The inlet is provided with a uniform velocity source and at the end termination impedance "$\rho_0 c_0 = 416.5\,\mathrm{kg\,m^{-2}\,s^{-1}}$" is applied to simulate the anechoic termination condition. The transmission loss is calculated using the inlet and outlet pressure and velocities, and the resulting expression is given as [1]

$$TL = 20\,\log\left|\frac{p_{in} + \rho_0 c_0 u_{in}}{2\rho_0 c_0 u_{out}}\right| \tag{43}$$

A mesh of 4750 elements with 5736 nodes was used for these calculations. Two times the maximum transverse dimension of the piston has been used as the length of the inlet and outlet duct in order to ensure that evanescent waves generated at the inlet and outlet decay out and only the plane waves exist. The existing mesh is valid up to a frequency of 5037 Hz, based on the assumption of a minimum of six elements per wavelength. The analysis is conducted from 10 to 3000 Hz in steps of 10 Hz. Computations are carried out by using laptop (Dell latitude D620 with 1 GB ROM). The computational time for analytical model for 300 frequency steps is 13 seconds including I/O, whereas the numerical model computational time is 105 seconds, excluding the pre- and post-processing time.

Fig. 2 shows that the transmission loss of a rectangular chamber calculated by the analytical method presented here tallies closely with that of the numerical model. Besides, the analytical method captures the higher-order modes effect very well.

4. Results and discussion

It may be noted that the transfer matrix parameters of all configurations shown in Fig. 1 are expressed in terms of the E-functions given by Eqs. (22) and (24); only marginal alterations are needed for different configurations. This is a marked simplification over the modal expansion method proposed in Ref. [4], which has been used here to validate the proposed Green's function method to calculate the transmission loss of the rectangular expansion chamber with different inlet and outlet configurations shown in Fig. 1.

Fig. 3 shows a comparison of the proposed method and the modal expansion method to calculate transmission loss for the reverse flow configuration shown in Fig. 1c. The results may be seen to agree very well throughout the frequency range. The dips in TL correspond to the higher-order mode excitation, as was observed in Ref. [9]. The asymmetric modes (1,0,0) and (1,0,1) are excited at 1133 and 1603 Hz, respectively. The dips at 2267 and 2534 Hz are due to the (2,0,0) and (2,0,1) modes, respectively.

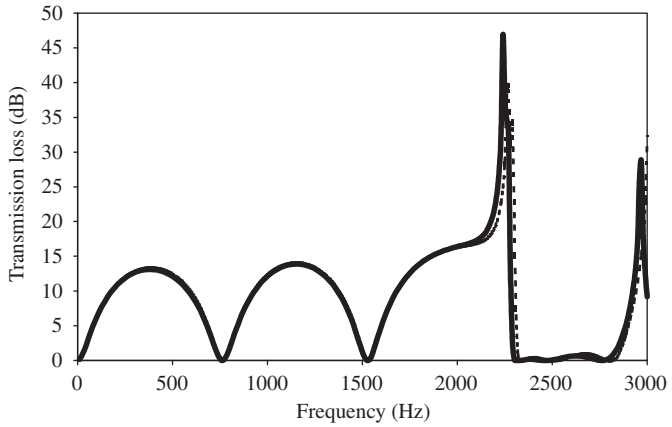

Fig. 2. Comparison of Green's function based method and the numerical model (FEM fluid) for a rectangular expansion chamber ($a = b = 0.15$ m, $a_1 = b_1 = a_2 = b_2 = 0.05$ m, centered configuration, and length $l = 0.225$ m). —— analytical method and ---- numerical model.

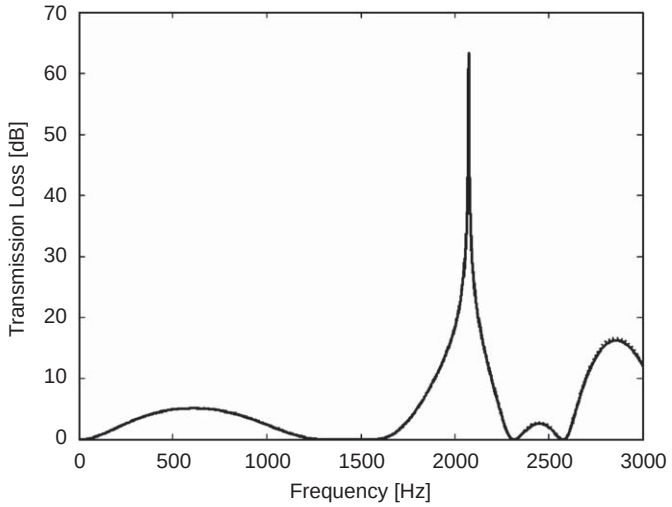

Fig. 3. Comparison of Green's function based method and the modal expansion method [4] for a reverse flow chamber ($a = b = 0.15$ m, $a_1 = b_1 = a_2 = b_2 = 0.025$ m, $a_{c1} = b_{c2} = 0.125$ m, $a_{c2} = b_{c1} = 0.025$ m, and length $l = 0.056$ m). —— Green's function method and ---- modal expansion method [4].

In Fig. 4, a comparison is made between the results of the centered inlet/outlet configuration with the offset inlet/outlet configuration, which shows deviation from the plane wave behavior at frequencies above 1000 Hz. In the centered inlet/outlet configuration, higher-order modes are generated at frequencies of 1800 Hz onwards. The same behavior is observed in the modal expansion method [4]. The offset configuration results show higher-order mode interaction with plane wave modes. The same observation has been made by Munjal with his collocation method [5]. Transverse modes of (1,0) (0,1) and (1,1) are not excited in the centered inlet/outlet configuration because the inlet/outlet ducts are located on the modes' nodal lines (zero pressure). However, the transverse modes (1,0) and (0,1) are excited in the off-set configuration at 1133 Hz.

Fig. 5 shows a comparison of the proposed method and the modal expansion method to calculate transmission loss of the EISO configuration (Fig. 1e). There is excellent agreement between the two methods for this configuration too. There is a peak in TL at 800 Hz due to the change in the outlet port location configuration from the centered inlet and outlet configuration, as shown in Fig. 3 with

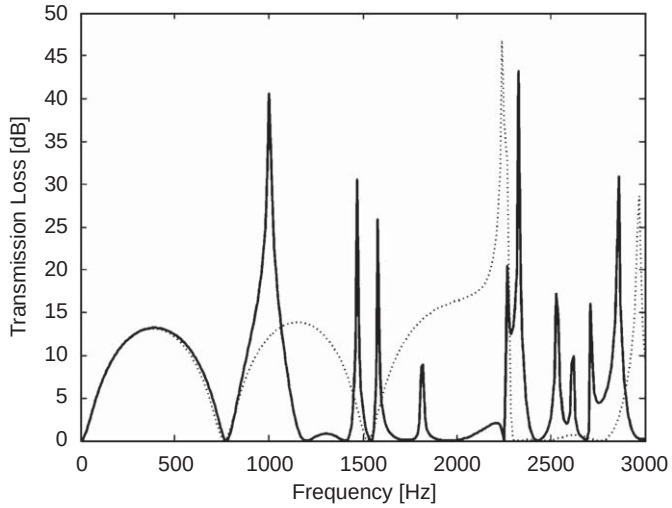

Fig. 4. Effect of the inlet and outlet port location in rectangular expansion chamber ($a = b = 0.15$ m, $a_1 = b_1 = a_2 = b_2 = 0.05$ m, centered configuration: $a_{c1} = b_{c2} = a_{c2} = b_{c1} = 0.075$ m and length $l = 0.225$ m, offset configuration: $a_{c1} = b_{c2} = 0.125$ m, $a_{c2} = b_{c1} = 0.025$ m). —— offset configuration and ---- centered configuration.

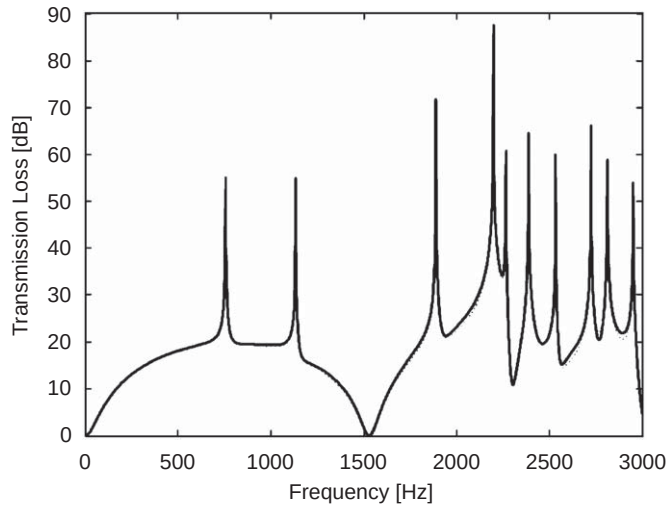

Fig. 5. Comparison of the transmission loss of the end-in/side-out rectangular chamber configuration ($a = b = 0.15$ m, $a_1 = b_1 = a_2 = b_2 = 0.05$ m, centered configuration: $a_{c1} = b_{c1} = a_{c2} = l_{c2} = 0.075$ m, and length $l = 0.225$ m). ---- Green's function method and —— modal expansion method [4].

$a_{c1} = b_{c1} = a_{c2} = l_{c2} =$ half of $a = b$. This is the tuned-chamber effect discussed in Refs. [10,11]. This configuration has an advantage of maintaining 20 dB of transmission loss over a larger frequency range.

Fig. 6 shows the Helmholtz resonator transmission loss including its 3-D effect for a thin neck length (Fig. 1g). In this case, there is a small deviation between the Ih's modal expansion method [4] and the proposed Green's function method. This may be due to the neglect of the evanescent modes in the Green's function method, which amounts to overlooking the end-correction effect.

Analytical transmission loss results, calculated for a rectangular chamber with one yielding wall, are shown in Fig. 7. It may be noted that the transmission loss values calculated by means of the proposed analytical model coincide very well with those of the numerical model. There is a small discrepancy between the two models near peaks in TL at 1180 and 1440 Hz. The computation time for 300 frequency steps is 1.75 minutes in the analytical model and 65 minutes in the numerical model, excluding pre- and post-processing. Thus, the

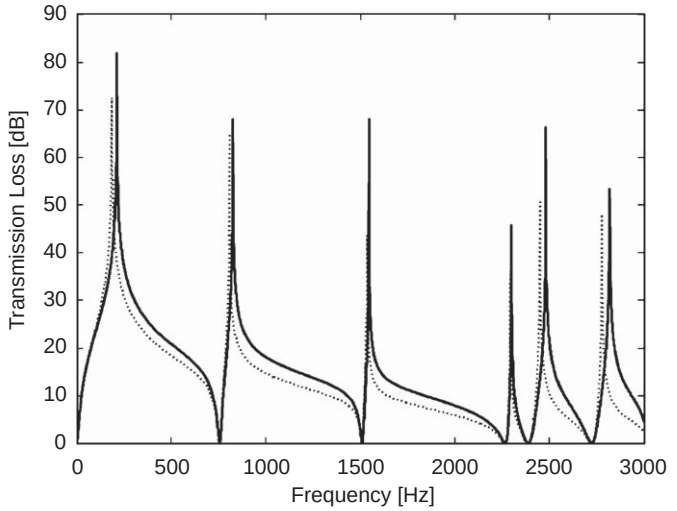

Fig. 6. Comparison of the two methods for prediction of transmission loss of a Helmholtz resonator ($a = b = 0.15\,\text{m}$, $a_1 = b_1 = 0.02\,\text{m}$, $a_{c1} = b_{c1} = 0.075\,\text{m}$, thin neck ($t_n = 0.001\,\text{m}$) and length $l = 0.225\,\text{m}$). ---- Green's function method and —— modal expansion method [4].

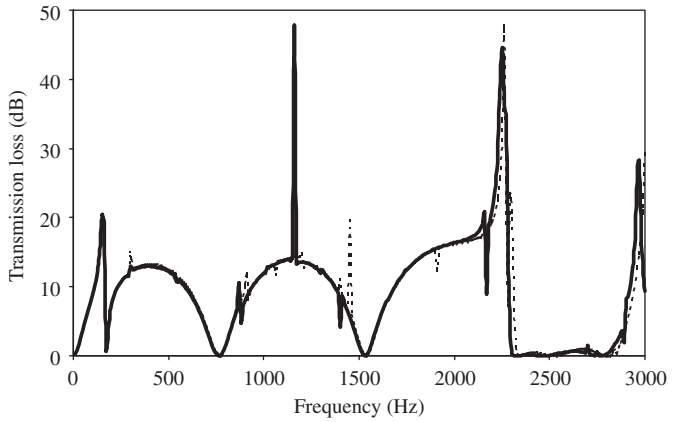

Fig. 7. Transmission loss of a rectangular chamber with a single yielding wall ($a = b = 0.15\,\text{m}$, $a_1 = b_1 = a_2 = b_2 = 0.05\,\text{m}$, $l = 0.225\,\text{m}$, centered configuration and 1 mm thick aluminum yielding wall). —— analytical method and ---- numerical model.

proposed model is computationally very efficient. The first N-curve near 160 Hz may be due to the coupling between the chamber and yielding wall. This indicates that at this frequency the energy is fluctuating between acoustic volume and structure. The structural–acoustic coupling plays a critical role in transmission loss prediction at low frequencies in a narrow-band region. The dips in TL curve of the analytical and numerical model coincide closely. Hence, the proposed analytical model would seem to be adequate for engineering applications.

5. Conclusions

An analytical method is proposed in this paper to predict the transmission loss as well as the four-pole parameters of rectangular rigid-wall expansion chamber for different inlet and outlet configurations, incorporating 3-D effects, and making use of Green's functions. This method is validated by means of the

FEM results and also the results available in the literature that make use of a modal expansion method, and is shown to be considerably simpler and more general than the latter.

The transfer matrices derived in this paper for different configurations are computationally more efficient than the corresponding numerical methods. The proposed analytical method illustrates the higher-order effects on TL curves that cannot be described by the classical plane wave theory. The derived transfer matrix may be combined with the transfer matrices of other constituent elements upstream and downstream in order to compute the overall transmission loss or insertion loss of the system. Thus, 3-D effects of an expansion chamber are taken into account while following 1-D theory in the remainder of the muffler.

The transfer matrix formulation of a rectangular chamber incorporating the flexibility of one of the chamber walls has been discussed and validated with the numerical models. The proposed model incorporates 3-D effects along with the acoustical and structural wave coupling phenomena.

Acknowledgments

The authors would like to thank GE Global Research, Bangalore and the Department of Science and Technology of the Government of India for providing the required resources for the research work reported here.

References

[1] M.L. Munjal, *Acoustics of Ducts and Mufflers*, Wiley, New York, 1987.
[2] J. Kim, W. Soedel, General formulation of four-pole parameters for three-dimensional cavities utilizing modal expansion, with special attention to the annular cylinder, *Journal of Sound and Vibration* 129 (2) (1989) 237–254.
[3] Y.-H. Kim, S.W. Kang, Green's solution of the acoustic wave equation for a circular expansion chamber with arbitrary locations of inlet, outlet port, and termination impedance, *Journal of the Acoustical Society of America* 94 (1) (1993) 473–490.
[4] J.G. Ih, The reactive attenuation of rectangular plenum chamber, *Journal of Sound and Vibration* 157 (1) (1992) 93–122.
[5] M.L. Munjal, A simple numerical method for three-dimensional analysis of simple expansion chamber mufflers of rectangular as well as circular cross-section with a stationary medium, *Journal of Sound and Vibration* 116 (1987) 71–88.
[6] P.M. Morse, K.U. Ingard, *Theoretical Acoustics*, McGraw-Hill, New York, 1968.
[7] S.M. Kim, M.J. Brennan, A compact matrix formulation using the impedance and mobility approach for the analysis of structural–acoustic systems, *Journal of Sound and Vibration* 223 (1) (1999) 97–113.
[8] SYSNOISE Rev 5.6, Users Manual, LMS International, 2003.
[9] C.I. Chu, H.T. Hua, I.C. Liao, Effects of three-dimensional modes on acoustic performance of reversal flow mufflers with rectangular cross-section, *Computers and Structures* 79 (2001) 883–890.
[10] M.L. Munjal, Plane wave analysis of the side inlet/outlet chamber mufflers with mean flow, *Applied Acoustics* 52 (2) (1997) 165–175.
[11] M.L. Munjal, A.G. Galaitsis, I.L. Ver, Passive silencers, in: I.L. Ver, L.L. Beranek (Eds.), *Noise and Vibration Control Engineering*, Wiley, New York, 2006 (Chapter 9).